DAMPING AND SOURCE STRENGTH CHARACTERISTICS OF CORRUGATED PIPES: INFLUENCE GAP WIDTH

S.P.C. Belfroid
TNO
Delft, The Netherlands

J. Golliard
CTTM
Le Mans, France

N. Gonzalez-Diez
TNO
Delft, The Netherlands

K. Lunde
Statoil ASA
Stavanger, Norway

S. Næss
Statoil ASA
Stavanger, Norway

ABSTRACT
To be able to predict the onset of flow induced pulsations in real risers, with variations in corrugation geometry and process conditions along the risers, a set of experiments was done with a variation of gap width and Reynolds number. In addition to configurations with constant cavity geometry also a geometry was tested in which the gap width varied. The damping, source strength and onset were determined via passive damping experiments and flow tests. The source strength was proportional to the (gap width)$^{1.55}$ and with the Reynolds number according (1+M)Re$^{0.25}$. The measured source strength of the varied geometry could be reconstructed from the power curves of individual cavities. That means no hydrodynamic interaction between cavities was observed in the geometries containing a mixture of different cavity geometries.

NOMENCLATURE
A	[-]	Dimensionless source strength
A_{pipe}	[m^2]	Pitch area
ID	[m]	Pipe diameter
L_{pitch}	[m]	Pitch length
M	[-]	Mach number
P	[W]	Acoustic Power
Re	[-]	Reynolds number
U	[m/s]	Flow velocity
W	[m]	Cavity width
k	[m]	Wave number
r_{up}, r_{down}	[m]	Up-, Downstream cavity edge radius
u'	[m/s]	Acoustic velocity
α	[m^{-1}]	Damping coefficient
ρ	[kg/m^3]	Density

Subscripts and superscripts
flow	Due to the flow
+	Quantity considered in direction of flow
-	Quantity considered in direction against flow

INTRODUCTION
Hoses with an internal corrugated profile are used in a large range of application. One of these is as flexible risers at offshore gas operations. Due to the inner corrugated profile, high amplitude tonal noise can be generated (for example [1]). The onset conditions of the sound generation is an interaction between sources and an energy balance between damping and amplification [1]. For pipes with all cavities the same geometry, the onset can be calculated using the energy balance (for long hose lengths) for which the amplification (source) and damping (viscous/thermal damping and losses due to reflection upstream and downstream) are determined via CFD or theoretically. However, in real systems, the geometry and conditions are not constant. The cavity width varies along the length due to manufacturing and installation stresses and compression on the carcass. In Figure 1, as an example, the variation in cavity width for a riser of 8" (28.6 m) is plotted. In addition to the geometry, also the conditions (density, velocity, viscosity (temperature) can vary along the riser due to frictional and gravitational effects.

Although the source and damping of an individual pitch can be calculated, this would be too time consuming for a complete riser. Therefore, scaling rules for the effect of the width and of the Reynolds number on the source strength and damping must

still be known. In addition, it must be verified that the cavities can be treated individually and that no interference occurs.

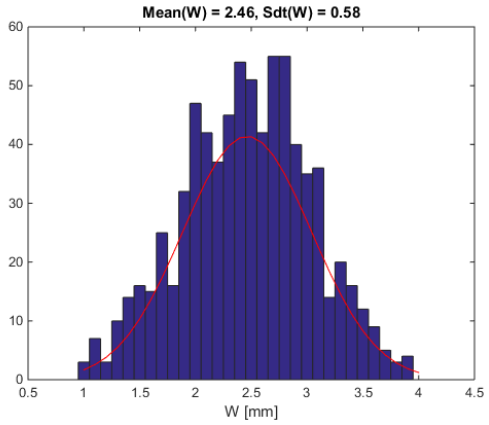

FIGURE 1: GAP WIDTH DISTRIBUTION 8"(28.6 m) LONG HORIZONTAL RISER.

In this paper a set of experiments is discussed in which, via passive damping measurement, the source strength and the thermal/viscous damping is measured for four different geometries at different velocities and pressures. Three geometries have a constant gap, one geometry has a variation in geometry.

PASSIVE DAMPING EXPERIMENT

With the passive damping experiments, the diffraction matrix is measured using two loudspeakers (Figure 2). For the details of the setup and the method it is referred to [2].

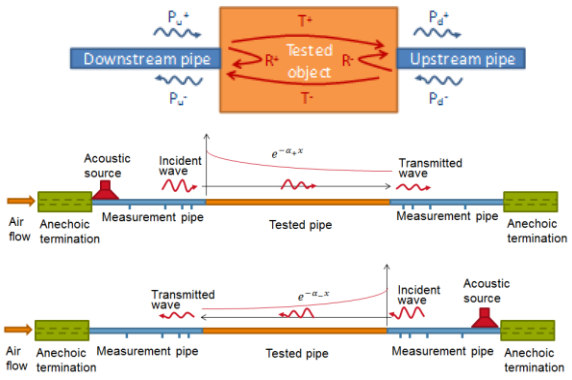

FIGURE 2: DEFINITIONS AND NOTATION FOR DIFFRACTION MATRIX OF TES OBJECT.BOTTOM: SCHEMATIC OF EXPERIMENTAL SETUP.

Important is to note, that the source strength is defined as the measured damping/amplification corrected for the measured damping at zero flow. This zero damping is corrected for convective effects. This leads to a measured dimensionless source power (generated in the flow and against the flow direction):

$$P^{+} = \frac{\langle P_{flow} \rangle}{\rho U A_{pipe} |u'|^2}^{+} = \frac{L_{pitch}}{4M^{+}} \cdot -Imag\left(k^{+} - \frac{k_{U=0}}{1+2M^{+}}\right) \quad (1)$$

$$P^{-} = \frac{\langle P_{flow} \rangle}{\rho U A_{pipe} |u'|^2}^{-} = \frac{L_{pitch}}{4M^{-}} \cdot -Imag\left(k^{-} - \frac{k_{U=0}}{1-2M^{-}}\right) \quad (2)$$

The total dimensionless source strength is the sum of the powers in both directions:

$$A = P^{+} + P^{-}$$

In the Mach number the speed of sound is the thermodynamic (c_0) speed of sound. In this the assumptions are made that the damping and amplification are small ($\alpha L << 1$) and that the upstream and downstream amplitudes are similar. These assumptions are not necessary but make the equations compact. In the analysis, these assumptions have not been made. For details (lengths, measuring locations) of the setup it is referred to [2].

EXPERIMENTS

Two sets of experiments have been performed. The first set are passive damping experiments. The second set consist of flow tests (with full reflective boundaries rather than the loudspeakers and dampers) to determine the onset conditions. As stated, four geometries have been measured in this campaign. All have a an internal diameter of 49 mm. The first three geometries are near identical except for the cavity width W. The fourth geometry is a more or less random combination of sections with a cavity width of 2.4, 3.6 and 4.8 mm ('random' geometry).

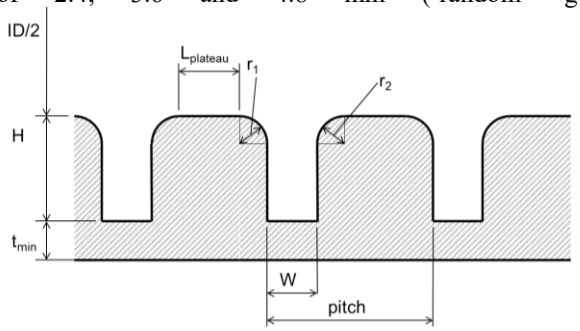

FIGURE 3: GEOMETRY DEFINITION.

Each geometry was measured at three pressures (1, 4, 6 bara) at different velocities. These velocities have been based on the expected onset velocity in a flow test, such that damping experiments were done at a velocity below and above onset conditions. The W = 1.2 and 2.4 mm geometry don't have an onset within the flow loop constraints. The 3.6 mm did have an onset velocity of 36, 13, 8 m/s at 1, 4 and 6 bara respectively.

All damping experiments have been done at an acoustic amplitude of approximal u'/U = 0.1% and of 1%. These results were near identical, indicating that the source is still in the linear regime at an amplitude of 1%. The source strength and peak Strouhal number are determined by taking a 2nd order polynomial fit through data in the bandwidth of ±0.1 around the peak Strouhal number. The definition used for the Strouhal number is:

$$Sr = f\frac{W+r_{up}}{U} \qquad (3)$$

The maximum of the fit is taken as the peak Strouhal and peak source strength (Figure 4). In the paper the source strength results are always plotted dimensionless.

TABLE 1: GEOMETRY DESCRIPTION (FIGURE 3 FOR DEFINITIONS).

Corrugated section length	3 [m]
Inner diameter (ID)	49 [mm]
Depth (H)	10.5 [mm]
Edge rounding (r1; r2)	1; 1 [mm]
Gap width (W)	1.2; 2.4; 3.6 [mm]
Plateau length L	13 [mm]
Pitch	16.2; 17.4; 18.6 [mm]

TABLE 2: TEST CONDITIONS.

W [mm]	Pressure [bara]	Velocity [m/s]
1.2	1; 4; 6	10; 20
2.4	1; 4; 6	10; 20
3.6	1 4 6	20, 40 5; 10; 20 5; 10

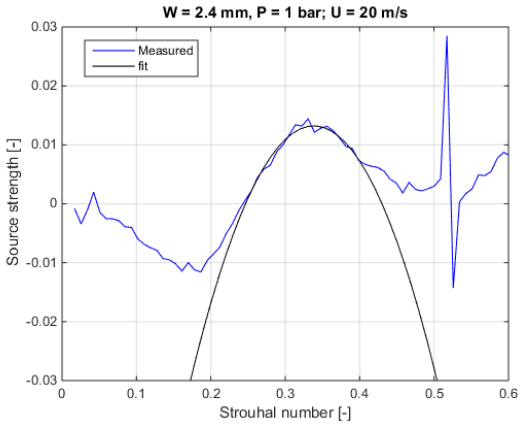

FIGURE 4: 2nd ORDER POLYNOMIAL FIT THROUGH MEASURED DATA.

BASE RESULTS - DAMPING

The viscous/thermal damping is measured at zero-flow for the three cases. In Figure 5, the measured damping is plotted as measured and relative to Kirchoff. For the three cases, the ratio to Kirchoff is not constant but increases with frequency. This is due to the reparative structure [3].

The differences between the three geometries are small with only at the higher frequencies a slightly lower measured damping for the W = 1.2 mm geometry. Practically, this means for a real riser, the width variations in a real riser can be ignored with respect to the damping. Considering the mean width seems sufficient.

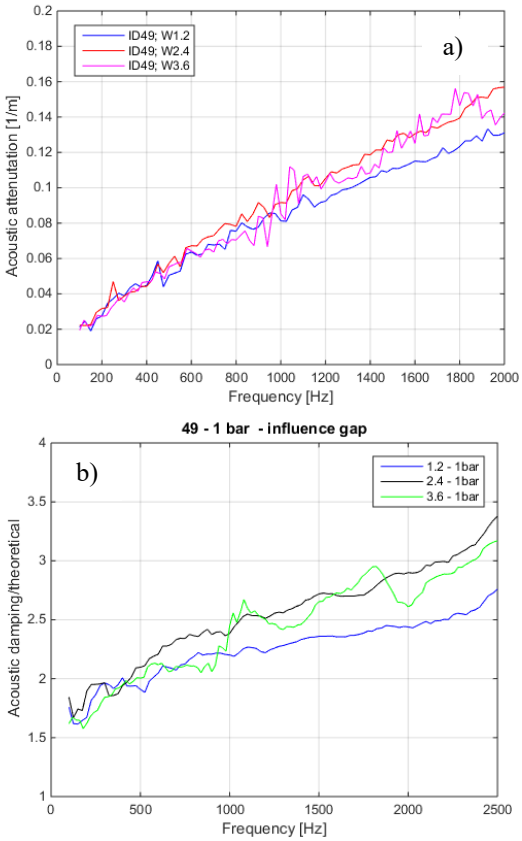

FIGURE 5: MEASURED DAMPING (a) AND RELATIVE TO KIRCHOFF (b) FOR SMOOTH PIPE AS FUNCTION OF FREQUENCY AT 1 bar.

SOURCE STRENGTH AS FUNCTION OF GAP

All base results are given in Table 3. For a fixed pressure and fixed velocities, the effect of gap width has been visualized in Figure 7. At all conditions the trend is a power proportionality according:

$$A \sim (W + r_{up})^{b} \qquad (4)$$

The power coefficient b is in that case approximately b= 1.55 but varies between 1.1 to 1.9 depending on flow conditions.

TABLE 3: OVERVIEW OF MEASURED STROUHAL AND DIMENSIONLESS SOURCE STRENGTH. W IS WIDTH [m]; P IS PRESSURE [bara]; U IS VELOCITY [m/s].

Case (W; P; U)	Sr [-]	Source strength [-]
1.2; 1; 10	0.30	0.0029
1.2; 1; 20	0.32	0.0092
1.2; 4; 10	0.30	0.0078

1.2; 4; 20	0.32	0.0119
1.2; 6; 10	0.30	0.0082
1.2; 6; 20	0.31	0.0118
2.4; 1; 10	0.34	0.0068
2.4; 1; 20	0.34	0.0132
2.4; 4; 10	0.35	0.0149
2.4; 4; 20	0.34	0.0175
2.4; 6; 10	0.34	0.0145
2.4; 6; 20	0.34	0.0195
3.6; 1; 20	0.37	0.0215
3.6; 1; 40	0.36	0.0310
3.6; 4; 5	0.38	0.0205
3.6; 4; 10	0.38	0.0227
3.6; 4; 20	0.38	0.0275
3.6; 6; 5	0.39	0.0230
3.6; 6; 10	0.38	0.0232

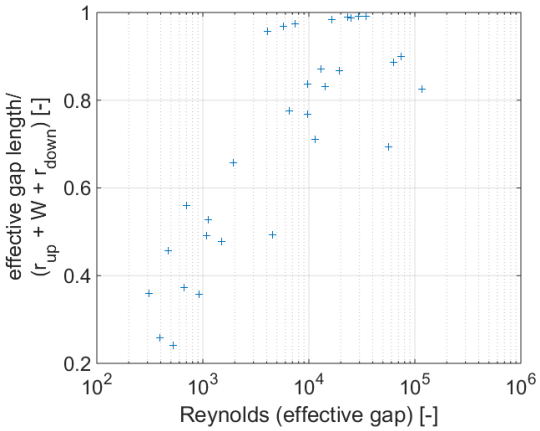

FIGURE 6: CALCULATED EFFECTIVE RELATIVE GAP LENGTH AS FUNCTION OF REYNOLDS NUMBER BASED ON EFFECTIVE GAP LENGTH.

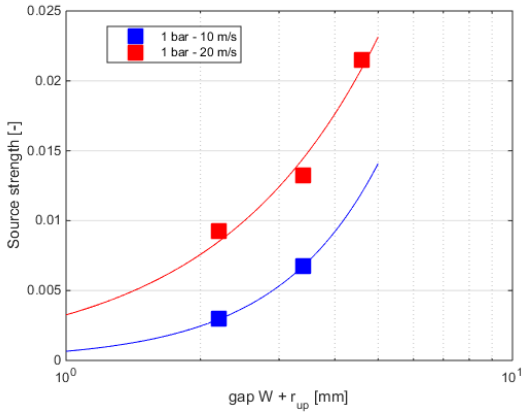

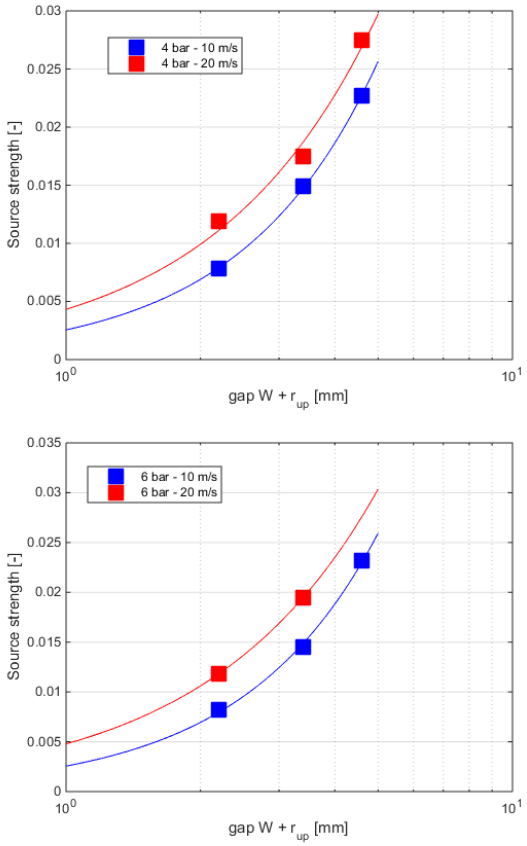

FIGURE 7: SOURCE STRENGTH AS FUNCTION OF GAP WIDTH AT FIXED PRESSURE AND VELOCITY CONDITIONS.

This variation is partly due to the choice in definition of the gap length W + r_{up}. An effective gap length has been determined to obtain a constant power coefficient b (minimized error). The effective gap seems to be dependent on the Reynolds number based on the gap length (Figure 6). This means that the power generating area is only the complete gap at high Reynolds numbers and that at lower Reynolds numbers, likely only the upstream part of the gap is effective.

SOURCE STRENGTH AS FUNCTION OF REYNOLDS NUMBER

In general, for cavity flow, at higher Reynolds numbers, the velocity gradient will steepen and therefore the source increase. In Figure 8, the source strength is plotted for the W = 3.6 mm cavity as function of Reynolds number for the three different pressures. There is on top of a clear Reynolds dependency also a clear absolute velocity component to the source strength.

The observed scaling has a linear component and a Reynolds dependency scaling. A scaling of:

$$A \sim (1 + M) Re^{b} \quad (5)$$

was found to fit all measurement data. In Figure 9, the scaled and measured source strength are compared to each other. The absolute velocity might have come in due to the convection

correction of the amplification/damping coefficient but why is unclear.

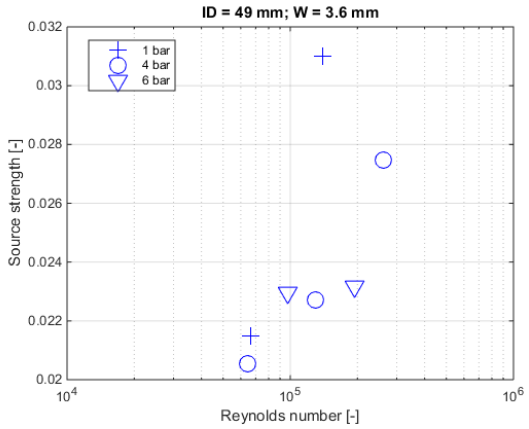

FIGURE 8: SOURCE STRENGTH W = 3.6 mm GEOMETRY AS FUNCTION OF REYNOLDS NUMBER.

The Reynolds dependency is a clear dependency on the velocity gradient at the wall. The power of 0.25 is the inverse proportionality of a smooth pipe wall friction (Blasius: $\lambda = 0.3164\ Re^{-0.25}$). A similar dependency has been found in CFD.

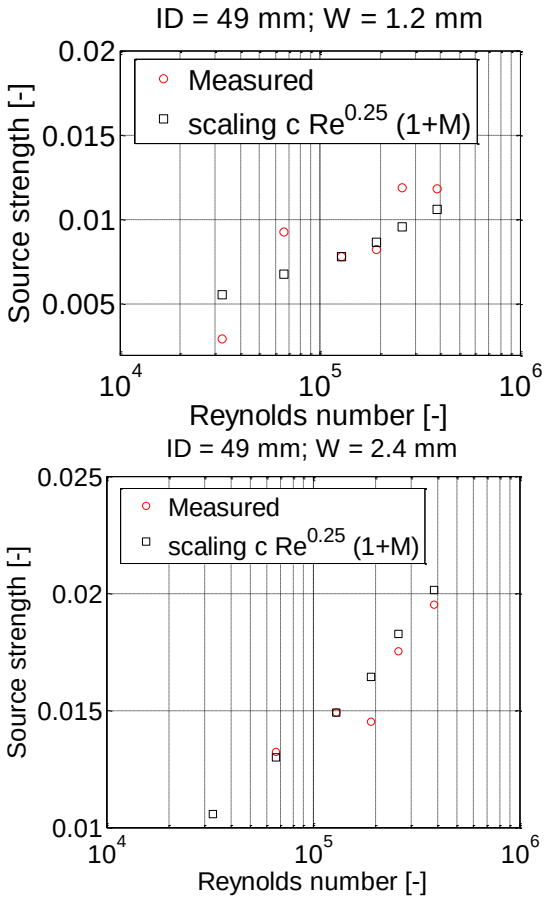

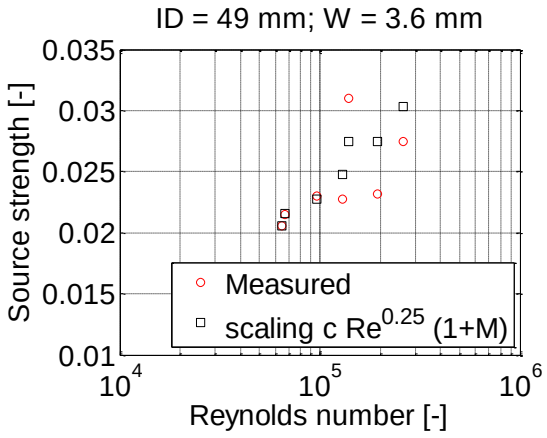

FIGURE 9: SCALING OF THE SOURCE STRENGTH FOR THE ID = 49 mm EXPERIMENTS.

RESULTS RANDOM GEOMETRY

Besides the constant geometry configurations, a 'random' geometry was tested (Table 4, results in table 5). This geometry consisted of 52 rings with a cavity width of W = 2.4 mm, 53 of W = 3.6 mm and 53 of W = 4.8 mm (leading to a total length of 2.97 m). The rings were more or less randomly distributed (each ring location is known). The goal of this pipe was to evaluate the effective source and Strouhal number in case of multiple variations of cavities. Complete mono-gap geometries with rings of W = 2.4 and 3.6 mm have been measured. Therefore, of these the source characteristics are known. The combination of 2.4, 3.6 and 4.8 mm was chosen based on the fact that a complete pipe with W = 2.4 mm did not have onset in a flow tests and a complete pipe with W = 3.6 mm did. Therefore, in this way also the onset velocities could be compared.

In comparison to the base case of W = 3.6 mm, the onset velocity is higher for the 'random' geometry (Table 6). Despite the fact that 1/3 of the cavities has a larger gap, this is almost completely compensated by the smaller gaps.

TABLE 4: TEST CONDITIONS 'RANDOM' GEOMETRY.

Pressure	Velocity
1 [bara]	10; 20 ; 40 [m/s]
4 [bara]	5; 10; 20 [m/s]
6 [bara]	5; 10; 20 [m/s]

TABLE 5: TEST RESULTS 'RANDOM'GEOMETRY. THE STROUHAL NUMBER IS BASED ON A LENGTH SCALE OF W = 3.6 mm (GAP = 3.6 + 1 = 4.6 mm).

Case	Strouhal [-]	Source [-]
1 bara		
10 m/s	0.35	0.0128
20 m/s	0.36	0.0174
40 m/s	0.34	0.0304

4 bara		
5 m/s	0.37	0.0146
10 m/s	0.36	0.0166
20 m/s	0.35	0.0246
6 bara		
5 m/s	0.37	0.0158
10 m/s	0.35	0.0191
20 m/s	0.35	0.0252

TABLE 6: COMPARISON ONET VELOCITY [m/s].

Pressure	W = 2.4 mm	W = 3.6 mm	Random
1 bar	56.1	36.0	40.1
4 bar	-	13.1	28.2
6 bar	-	8.0	13.5

For the conditions (P;U) = (6,10), the measured source strength is plotted for the W = 2.4, 3.6 and the random geometry. The random geometry results are in Strouhal close to the W = 2.4 and in terms of source strength (peak power) between the 2.4 and 3.6 geometry.

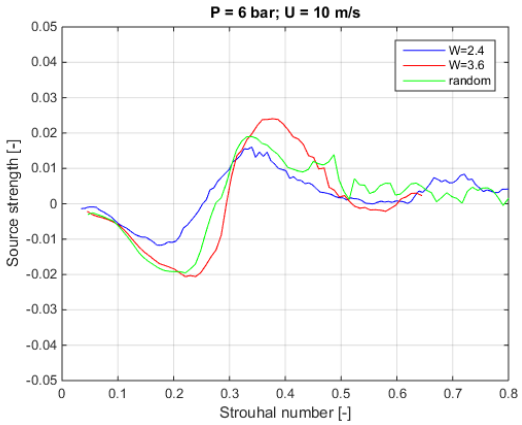

FIGURE 10: SOURCE STRENGTH AS FUNCTION OF STROUHAL NUMBER. THE STROUHAL NUMBER FOR THE RANDOM GEOMETRY IS BASED ON A LENGTH SCALE OF W = 3.6 mm (GAP = 3.6 + 1 = 4.6 mm).

To explain this, the random geometry source power is reconstructed. Focus was on the positive part of the source power spectrum. The random curve is reconstructed based on the measured curves of the W = 2.4 mm and W = 3.6 mm geometries. The W = 4.8 mm cavities are based on a scaled curves. The W = 3.6 mm curve is translated to the 4.8 mm, based on the scaling $A \sim (W+r_{up})^{1.55}$. The peak Strouhal number for the W = 4.8 mm is based on the scaling of $Sr \sim (ID/(W+r_{up}))^{-0.2653}$ found in earlier tests.

The resulting curve is obtained by adding the contributors of each pitch and dividing by the number of pitches (52 + 53 + 53). In Figure 11, all the curves are compared. The comparison between the measured and reconstructed cavity is very good in both peak Strouhal and peak amplitude. This confirms that each cavity can be treated individually and almost no hydrodynamic interference occurs. Also the more flattened profile at higher Strouhal number compares well to the actual measurements.

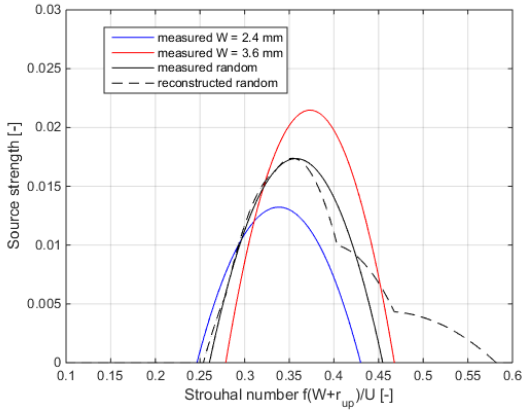

FIGURE 11: MEASURED AND RECONSTRUCTED POWER CURVES. THE MEASURED CURVES ARE 2nd ORDER POLYNOMIAL FITS OF THE MEASURED SIGNALS.

CONCLUSIONS AND DISCUSSION

A set of four geometries have been tested both using the passive damping technique and flow tests to determine the scaling rules for gap width and Reynolds number of the source strength of cavities in a corrugated pipe.

For the dependence of source strength on the gap width a scaling is found according to:

$$A \sim (W + r_{up})^{b} \quad (6)$$

With a geometry in which the cavities have been varied, the scaling effects have been verified. In the same experiments it was shown that the combination of different gaps can be modelled as the summation of individual contributions and that no hydrodynamic interference is present. For the dependence of the source strength on the Reynolds number, a scaling is found of:

$$A \sim (1 + M) Re^{0.25} \quad (7)$$

ACKNOWLEDGMENTS

The authors would like to thank Statoil for allowing publishing this material and the help of Yves Auregan (Le Mans) in both the experiments and the analysis.

REFERENCES

[1] Belfroid, S.P.C., Golliard, J., Korst, H., 2013, 'Prevention of pulsations caused by flexible risers', ATCE New Orleans, USA, SPE-166424-MS.

[2] Golliard, J. et.al, 2015, Direct measurements of acoustic damping and sound amplification in corrugated pipes with flow', ASME-PVP Boston, USA, PVP2015-45494

[3] Del Giudice, S., Bernasconi, G., 2013, Acoustic response of a sinusoidally perturbated hard-walled duct', Mathematical Problems in Engineering, 2013, 1-6